Indian Journal of Chemical Technology
Vol. 32, March 2025, pp. 176-189
DOI: 10.56042/ijct.v32i2.15276

MHD radiative Williamson nanofluid through Darcy Forchheimer medium due to stretching sheet in the presence of heat source, activation energy and motile microorganisms

M. Vinodkumar Reddy[1], Tusar Kanti Das[2], K. Malleswari[1], Jintu Mani Nath[3*], S. Saroja[1] & V. Madhusudana Reddy[4]

[1]Department of Mathematics, Malla Reddy Engineering College (Autonomous), Medchal, Secunderabad-500100, India

[2]Department of Mathematics, Dudhnoi College, Assam-783124, India

[3]Department of Mathematics, Mangaldai College, Mangaldai-784125, India

[4]Department of Electrical and Electronics Engineering, Malla Reddy Engineering College (Autonomous), Medchal, Secunderabad-500100, India

*E-mail: jmnath1995@gmail.com

Received 24 November 2024; accepted 10 February 2025

The study investigates the magneto radiative flow of Williamson nanofluid with entropy generation in Darcy Forchheimer porous medium over a stretching sheet with motile microorganisms and activation energy. The Brownian motion, thermophoresis, chemical reaction, heat source and suction/injection are also taken into this flow model. The set of partial differential equations (PDEs) in the mathematical framework is simplified to ordinary differential equations (ODEs) by employing the similarity transformation. Computational outcomes are obtained using a Runge-Kutta based shooting technique implemented via the BVP5C MATLAB package. The research illustrates graphical representations elucidating the influence of various dimensionless parameters on flow regime. The main findings indicate that the escalating velocity profile is observed with magnetic field and Darcy-Forchheimer number. Also, an escalation in the Brinkman number and magnetic field increases the entropy generation. The motile microorganism profile is reduced for enlarging values of the bio-convection Lewis number and Peclet number. Furthermore, the thermal efficacy rate in the proximity of the surface is significantly touched up by the enhancing Brownian motion, radiation and suction factor and the proximity solutal transfer rate exhibits elevation with escalating Schmidt and chemical reaction. Implications entail the refinement of thermal exchange and cooling mechanisms employing nanofluids to bolster efficacy and environmental viability.

Keywords: Bioconvection, Chemical reaction, Darcy-Forchheimer, Entropy generation, MHD, Motile microorganisms, Nanofluid, Thermal radiation, Williamson fluid

Introduction

Nanofluids characterize a model transferal in fluid dynamics, integrating nanoparticles, nano-scale entities, into regular fluids. The primary objective is to optimize heat conductivity via precise nanoparticle dispersion and stabilization within the fluid matrix. This engineering finesse escalates thermal transport mechanisms, exploiting nanofluids' outstanding thermal attributes. Nanofluids find applications in numerous domains, such as chemical science, environmental science, electronics, nuclear systems, industrial processes, and bio-medical science. Scholarly research underscores nanofluids' pivotal role in catalyzing innovation across these disciplines, exemplifying their indispensable contributions to contemporary scientific endeavours.

Choi et al.[1] of Argonne National Laboratory initially put forward the prospect of these tiny fluids in 1995. Relying on their computational research, Adnan et al.[2] found that nanofluids including silver nanostructures had better thermal transfer efficiency than those containing Nano dimensions alone. Abbas et al.[3] explored the thermodynamic traits of second-grade nanofluid movement incorporating radiation and chemical reaction via a slender stretching sheet. Furthermore, Paul et al.[4] examined the magnetohydrodynamic hybrid-nanofluid flow in a porous medium across a vertically stretching cylinder with heat stratification impact. Recently, some other significant inquiries into nanofluids exhibiting various tangible characteristics are mentioned in the publications [5-7].

MHD Williamson fluid, a magnetohydrodynamic medium, showcases non-Newtonian attributes typified by a power-law correlation between stress and strain rate. Its utility extends to simulating complex fluid dynamics over various domains like geophysics, astrophysics, and engineering, where conventional Newtonian fluids inadequately represent complex flow phenomena. Asjad et al.[8] addressed the consequence of activation energy and MHD on Williamson fluid movement in the existence of bioconvection. After that, Saravana et al.[9] explored the heat radiation and diffusion influences in magneto-Williamson and Casson fluid flows through a slender stretching surface. Also, Khan et al.[10] investigated the heat and Mass transmission analysis for Williamson MHD nanofluid flow via a stretched sheet. Recently, Jangid et al.[11] explored the heat and mass transportation of hydromagnetic Williamson nanofluid movement over an exponentially stretched surface incorporating the impacts of suction/injection, buoyancy, radiation, and chemical reaction.

The Darcy-Forchheimer flow model in porous media is pivotal in fluid dynamics, offering significant insights into fluid motion within porous substrates. It integrates Darcy's classic formulation for laminar flow in porous media with Forchheimer's extension, accommodating non-linear phenomena like inertial resistance and turbulence. Its relevance spans domains involving geosciences, petroleum, and environmental engineering, and industrial filtration. From analyzing groundwater dynamics to optimizing oil recovery and facilitating environmental remediation, the model aids in enhancing the efficiency of industrial filtration systems. The Darcy-Forchheimer framework serves as an indispensable tool for advancing scientific understanding and engineering applications in porous media. Sharma and Gandhi[12] investigated the mixed impacts of Joule heating and uneven thermal source/sink on unsteady MHD mixed convective movement via a vertical stretching surface embedded in a Darcy-Forchheimer porous medium. Also, Jawad et al.[13] computationally performed a study on chemically reacting Darcy-Forchheimer flow of Buongiorno Maxwell fluid incorporating activation energy in the presence of nanoparticles. Moreover, Zafar et al.[14] conducted an irreversibility analysis of the radiative movement of Prandtl nanofluid over a stretched surface in a Darcy-Forchheimer medium with activation energy and chemical reaction. Recently, Awais et al.[15] examined the influences of viscous dissipation and activation energy for the MHD Eyring-Powell fluid flow integrating the Darcy-Forchheimer and variable fluid properties.

The incorporation of motile microorganisms into nanofluidic environments presents an intriguing interdisciplinary frontier with broad practical implications. These microorganisms, proficient in navigating fluidic media, inject dynamism into nanofluid dynamics. Their interaction with nanoparticles dispersed in the fluid significantly influences the flow patterns, thermal transfer, and mass transmission phenomena. This phenomenon finds applications in biotechnology, optimizing biofuel production and environmental remediation, environmental engineering for efficient wastewater treatment systems, and biomedical sciences for targeted drug delivery and diagnostics.

Haq et al.[16] theoretically inspected the gyrotactic microorganisms in radiated nanomaterial Williamson fluid incorporating activation energy. Also, Song et al.[17] explored the irregular stretched flow of Williamson nanofluid along swimming of motile gyrotactic microorganisms. Awan et al.[18] investigated the bio-convection influences on Williamson nanofluid flow with exponential thermal source and motile microorganism across a stretching sheet. Furthermore, Hussain et al.[19] studied the magneto-bioconvection chemically reactive movement of radiative Williamson nanofluid integrating oxytactic situation of microorganisms. Recently, Kamal et al.[20] explored the second law analysis of two-phase Maxwell mixed convective nanofluid employing marangoni flow and gyrotactic microorganisms.

Activation energy, pivotal in chemical kinetics, denotes the energy threshold required for a reactant molecule to transition into a product. Coined by Svante Arrhenius, it governs reaction kinetics, elucidating the energetic barrier for reaction initiation. Vital in hyperthermia therapy for cancer treatment, it optimizes cell death induction temperatures via dosimetry. Crucial in drug formulation and stability testing, it also aids in food preservation. Hamid and Khan[21] investigated the influences of binary chemical reactions integrating activation energy on the unsteady movement of magneto-Williamson nanofluid. Also, Dhlamini et al.[22] studied the activation energy and binary chemical reaction impacts in combined convective nanofluid flow incorporating Newtonian heating. Moreover, in the flow of Prandtl–Eyring nanofluid, Khan et al.[23] analyzed the entropy generation optimization integrating the binary chemical reaction and Arrhenius activation energy. Recently, Vijayalakshmi et al.[24] inspected the impacts of chemical Reaction and Activation Energy on the Riga plate that emerged in a porous medium via a Maxwell fluid flow.

Entropy generation in fluid flow signifies the irreversible enhancement in entropy due to inherent dissipative processes within the fluidic environment. It is pivotal in understanding the thermodynamic intricacies of fluid dynamics, guiding engineers to optimize designs, reduce energy dissipation, enhance thermal conduction, and improve overall system efficiency. This paradigm applies to diverse domains including heat exchange, turbine operation, chemical synthesis, and environmental remediation. The analysis of entropy optimization on MHD radiative transport of Williamson nanofluid in the presence of viscous dissipation and chemical reaction was performed by Kumar et al.[25]. Butt et al.[26] computationally investigated the magnetic field impacts on entropy generation in viscous flow via a stretching cylinder. Also, Baag et al.[27] explored the entropy generation analysis for magneto-viscoelastic movement across a stretching sheet incorporating a porous medium. Moreover, Khan et al.[28] investigated the entropy generation minimization and binary chemical reaction integrating activation energy in the radiative flow of nanomaterial. Ullah et al.[29] inspected the thermal transport assessment along entropy generation and heat density impacts on boundary layer movement of magneto nanofluid via the stretching sheet. Hussain et al.[30] analyzed the entropy optimization in the bio-convective chemically reactive flow of micropolar nanomaterial. Recently many researchers[31-33] numerically investigated the flow of nanofluid incorporating various impacts.

Motivated by the above-mentioned literature, an attempt is made to examine the magneto Darcy Forchheimer flow of bioconvective Williamson nanofluid over a stretched sheet with entropy generation, activation energy, and motile microorganism. Also, incorporating thermal radiation, suction/ injection, and heat source impact provides the distinctiveness of this research. This gives the required novelty of this research. This study aims to provide a unique and innovative approach to understanding these complex phenomena. The resulting governing equations are computationally solved using the BVP5C built-in MATLAB package. With so many practical applications and an entirely novel trajectory for the field, this work attracts academics and industry specialists eager to apply these innovative findings to promote innovation and efficiency in an assortment of manufacturing processes.

Mathematical formulation

Examine the entropy optimization of Williamson nanofluid in a magneto Darcy Forchheimer flow towards a stretched sheet with motile microorganisms on it through injection/suction. Brownian motion, thermophoresis, radiation and heat sources have all been discussed in connection to the thermal equation. Chemical reaction and activation energy are also taken into consideration. The representation flow configuration for the current flow model is shown in Fig. 1. In meanwhile, the sheet that borders the flow problem is susceptible to flow in the x direction, whereas the y direction is perpendicular to it. Assumed that linear velocity of the stretching sheet is $u_w = ax$. The sheet uniform thermal and concentration are to be T_w and C_w, whereas the ambient temperature and concentration are T_∞ and C_∞, respectively. Considering the aforementioned assumptions, the governing equations for flow are [18,25]:

$$\frac{\partial u}{\partial x} + \frac{\partial v}{\partial y} = 0 \qquad \text{... (1)}$$

$$u\frac{\partial u}{\partial x} + v\frac{\partial u}{\partial y} = \upsilon\frac{\partial^2 u}{\partial y^2} + \sqrt{2}\upsilon\Gamma\frac{\partial u}{\partial y}\frac{\partial^2 u}{\partial y^2} - \frac{\sigma B_0^2 u}{\rho} - \frac{\mu}{\rho k_1}u - \frac{c_b}{\sqrt{k_1}}u^2 \qquad \text{... (2)}$$

$$u\frac{\partial T}{\partial x} + v\frac{\partial T}{\partial y} = \alpha\frac{\partial^2 T}{\partial y^2} + \left(\frac{\mu}{\rho C_P}\right)\left(\frac{\partial u}{\partial y}\right)^2 + \left(\frac{\mu}{\rho C_P}\right)\Gamma\left(\frac{\partial u}{\partial y}\right)^3 + \tau\left(D_B\frac{\partial c}{\partial y}\frac{\partial T}{\partial y} + \frac{D_T}{T_\infty}\left(\frac{\partial T}{\partial y}\right)^2\right) - \frac{1}{\rho C_P}\frac{\partial q_r}{\partial y} + \frac{Q_o}{\rho C_P}(T - T_\infty) + \frac{\sigma\beta_0^2}{\rho C_P}u^2 \qquad \text{... (3)}$$

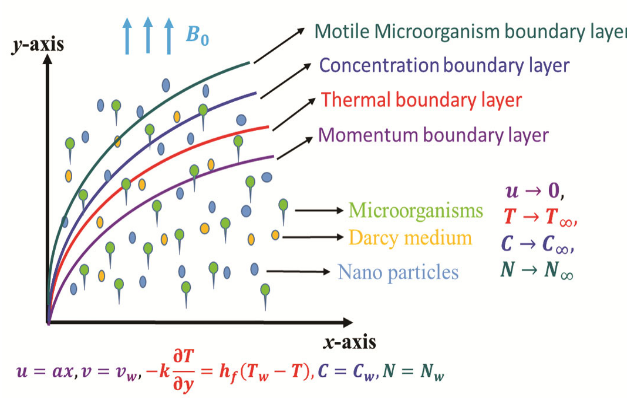

Fig. 1 — Flow geometry

$$u\frac{\partial C}{\partial x}+v\frac{\partial C}{\partial y}=D_B\frac{\partial^2 C}{\partial y^2}+\frac{D_T}{T_\infty}\frac{\partial^2 T}{\partial y^2}-K_r{}^2(C-C_\infty)\left(\frac{T}{T_\infty}\right)^n exp\left(\frac{-E_a}{kT}\right) \quad \text{... (4)}$$

$$\left(u\frac{\partial N}{\partial x}+v\frac{\partial N}{\partial y}\right)=D_m\frac{\partial^2 N}{\partial y^2}-\frac{bw_c}{(C_w-C_\infty)}\frac{\partial}{\partial y}\left(N\frac{\partial C}{\partial y}\right) \quad \text{... (5)}$$

The considered boundary conditions as:

$$u=u_w\,,v=v_w\,,\frac{\partial T}{\partial y}=\frac{-h_f}{k}(T_w-T)\,,C=C_w\,,N=N_w\;at\;y=0$$
$$u\to 0,T\to T_\infty\,,C\to C_\infty\,,N\to N_\infty\;\;as\;y\to\infty \quad \text{... (6)}$$

The similarity transformations are introduced as follows[18,25]:

$$u=axf'(\eta)\,,v=-(a\upsilon)^{\frac{1}{2}}f(\eta)\,,\eta=\sqrt{\frac{a}{\upsilon}}\,y\,,$$
$$\theta(\eta)(T_w-T_\infty)=T-T_\infty\,,\phi(\eta)(C_w-C_\infty)=C-C_\infty\,,\chi(\eta)(N_w-N_\infty)=N-N_\infty \quad \text{... (7)}$$

Using similarity transformations in Eqs (2) - (6) simplified to

$$(1+Wef'')f'''-(M+K)f'++ff''-Frf'^2-f'^2=0 \quad \text{... (8)}$$

$$\left(1+\frac{4}{3}R\right)\theta''+Pr\left[f\theta'+Nb\theta'\phi'+Nt\theta'^2+MEcf'^2+Ecf''^2+\frac{1}{\sqrt{2}}EcWef''^3+Q\theta\right]=0 \quad \text{... (9)}$$

$$\phi''+Scf\phi'+\left(\frac{Nt}{Nb}\right)\theta''-Sc\,Cr\,(1+\alpha_1\theta)^n exp\left(\frac{-E}{1+\alpha_1\theta}\right)\phi=0 \quad \text{... (10)}$$

$$\chi''+Lb\,f\chi'-Pe[(\delta_1+\chi)\phi''+\chi'\phi']=0 \quad \text{... (11)}$$

The corresponding boundary conditions as:

$$f(0)=S,f'(0)=1,\theta'(0)=Bi(\theta(0)-1),\phi(0)=1,\chi(0)=1$$
$$f'(\infty)=0,\theta(\infty)=0,\phi(\infty)=0,\chi(\infty)=0 \quad \text{... (12)}$$

where,

$$M=\frac{\sigma B_\circ^2}{\rho a}\,,\;K=\frac{\upsilon}{ak_1}\,,\;We=\Gamma u_w\sqrt{\frac{2a}{\upsilon}}\,,\;Fr=\frac{c_b}{\sqrt{k_1}}$$
$$,\;R=\frac{4\sigma^* T_\infty^3}{k^* k}\,,\;Pr=\frac{\upsilon}{\alpha}\,,\;Q=\frac{Q_\circ}{\rho C_p a}\,,$$
$$Ec=\frac{u_w^2}{\left(T_w-T_\infty\right)C_p}\,,\;Nb=\frac{\tau D_B\left(C_w-C_\infty\right)}{\upsilon}\,,$$
$$Nt=\frac{\tau D_T\left(T_w-T_\infty\right)}{T_\infty\upsilon}\,,\;Sc=\frac{\upsilon}{D_B}\,,\;Cr=\frac{K_r}{a}\,,$$
$$Lb=\frac{\upsilon}{D_m}\,,\;S=-\frac{v_w}{\sqrt{a\upsilon}}\,,\;Bi=\frac{h_f}{k}\sqrt{\frac{\upsilon}{a}}\,.$$

The skin friction, Nusselt number, Sherwood number, Motile density number demonstrated as follows:

$$\sqrt{Re_x}C_f=\left(1+\frac{We}{2}\right)f''(0),\frac{Nu}{\sqrt{Re_x}}=-\left(1+\frac{4}{3}R\right)\theta'(0),$$
$$\frac{Sh}{\sqrt{Re_x}}=-\phi'(0)\,,\frac{Nh}{\sqrt{Re_x}}=-\chi'(0) \quad \text{... (13)}$$

Analysis of Entropy generation

The volumetric entropy generation of magneto-Williamson nanofluid is defined as:

$$Ns=\alpha_1\left(1+\frac{4}{3}R\right)\theta'^2+Br\left(f''^2+\frac{We}{\sqrt{2}}f''^3\right)+L_1\left(\frac{\alpha_2}{\alpha_1}\right)\phi'^2+Br(M+K)F'^2+L_1\theta'\phi'+L_2\left(\frac{\alpha_3}{\alpha_1}\right)\chi'^2+L_2\chi'\theta' \quad \text{... (14)}$$

in which,

$$\alpha_1=\frac{\Delta T}{T_\infty},L_1=\frac{RD(C_w-C_\infty)}{k}\,,L_2=\frac{RD(N_w-N_\infty)}{k}\,,We=\Gamma u_w\sqrt{\frac{2a}{\upsilon}},$$
$$\alpha_2=\frac{\Delta C}{C_\infty},\alpha_3=\frac{\Delta N}{N_\infty},Br=\frac{\mu_0 u_w^2}{k\Delta T} \quad \text{... (15)}$$

are the temperature difference parameter, diffusion parameter due to concentration, diffusion parameter due to microorganisms, Williamson fluid, concentration difference parameter,concentration difference of microorganisms and Brinkman number respectively.

Numerical solution

The resulting Eqs (8) - (11) and BCs (12) are particularly difficult to solve analytically because they are higher-order, linked nonlinear. The resulting equations are numerically solved using BVP5C built-in MATLAB package. To use this technique, we propose the following substitutions:$f_1=f\,,f=f'\,,f_3=f''\,,\;f_4=\theta\;,\;f_5=\theta'\,,\;f_6=\;\phi\;,\;f_7=\;\phi'\,,F_8=\chi\,,F_9=\chi'$. The reduced equations assume the below form:

$$f_1' = f_2, \quad \dots (16)$$

$$f_2' = f_3, \quad \dots (17)$$

$$f_3' = \left(\frac{1}{(1+Wef_3)}\right)[(M+K)f_2 - f_1f_3 + Frf_2f_2 + f_2f_2], \quad \dots (18)$$

$$f_4' = F_5, \quad \dots (19)$$

$$f_5' = \frac{1}{\left[1+\frac{4}{3}R\right]}\left(Pr\left[-f_1f_5 - Qf_4 - Nbf_5f_7 - Nt\,f_5f_5 - MEc\,f_2\,f_2 - Ecf_3\,f_3 - \frac{1}{\sqrt{2}}EcWe\,f_3\,f_3\,f_3\right]\right), \quad \dots (20)$$

$$F_6' = F_7, \quad \dots (21)$$

$$f_7' = -\frac{Nt}{Nb}\left[\frac{1}{\left[1+\frac{4}{3}R\right]}\left(Pr\left[-f_1f_5 - Qf_4 - Nbf_5f_7 - Nt\,f_5f_5 - MEc\,f_2\,f_2 - Ecf_3\,f_3 - \frac{1}{\sqrt{2}}EcWe\,f_3\,f_3\,f_3\right]\right)\right] - Scf_1f_7 + ScCr(1+\alpha_1f_4)^n exp\left(\frac{-E}{1+\alpha_1f_4}\right)f_6 \quad \dots (22)$$

$$f_8' = f_9, \quad \dots (23)$$

The appropriate boundary conditions are:

$$f_1 = S,\ f_2 = 1,\ f_5 = Bi(f_4 - 1),\ f_6 = 1\ ,\ f_8 = 1\ at\ \eta = 0, \quad \dots (24)$$

$$f_2 = 0,\ f_4 = 0,\ f_6 = 0,\ f_8 = 0\ as\ \eta \to \infty. \quad \dots (25)$$

Results and Discussion

Figs 2 and 3 elucidate the impact of the magnetic parameter, on the velocity and thermal profiles, respectively. An escalation in the magnetic effect precipitates a continuous diminution in the flow velocity across the entire flow domain, but the converse trend can be seen in temperature due to the Lorentz force which causes a reduce in velocity and rise in temperature. Fig. 4 demonstrates the influence of porosity on velocity profiles. The porosity parameters, K is inversely related to the diameter of the porous space; as K increases, the diameter decreases. This reduction in space heightens resistance to the fluid flow within the porous medium. Consequently, the fluid encounters increased resistance, leading to a marked decrease in velocity. The elevated resistance, driven by the porosity parameter, significantly impedes fluid movement

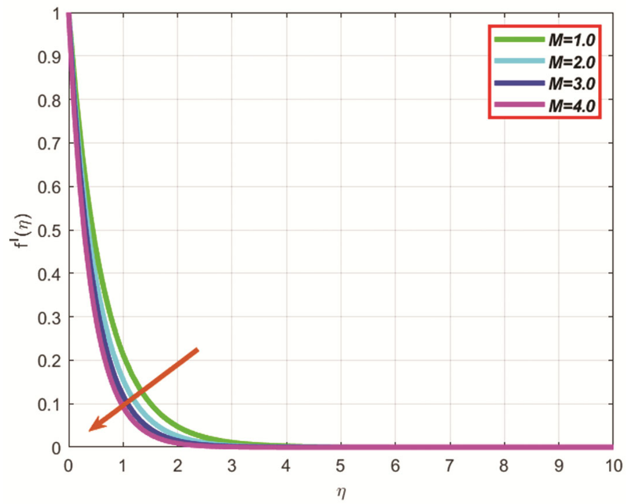

Fig. 2 — Plot of f' (η) with various values of M

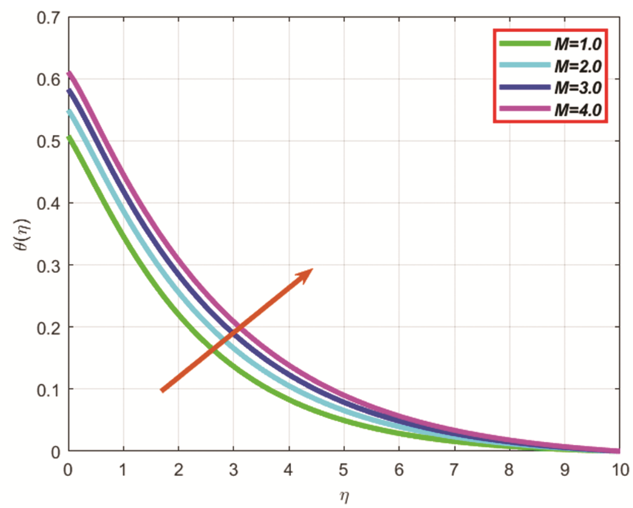

Fig. 3 — Plot of θ(η) with various values of M

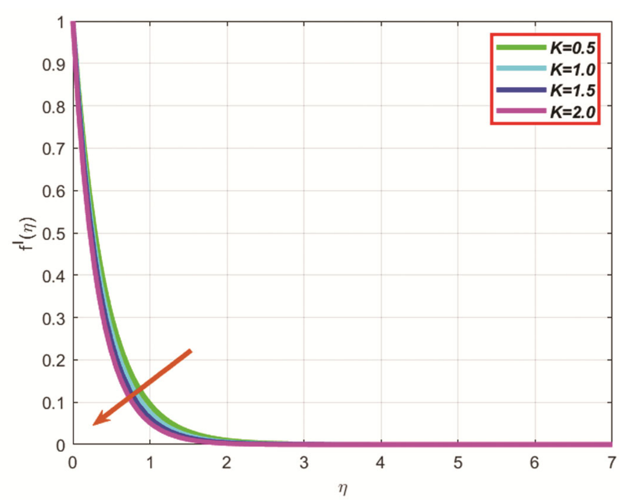

Fig. 4 — Plot of f' (η) with various values of K

through the porous region, resulting in a notable reduction in velocity.

Fig. 5 illustrates the significance of the Darcy-Forchheimer inertia factor on the velocity distribution profile. The inertia factor is inherently associated with medium permeability and drag coefficient. Thus, fluid velocity diminishes greater inertia. With the higher value of Fr, the porosity and drag coefficient of the medium is further enhanced so that it resists more to the flow of that fluid. Thus the liquid is further delayed, reducing the velocity with greater Forchheimer factor. The preceding relationship quantifies the influence of the inertia timescale with respect to fluid flow in porous media and shows the negative relationship between fluid velocity. As the Eckert number rises, the thermal profile increases, as shown in Fig. 6. As this number increases, the enthalpy differences gradually decrease which is a clear indication of the greater diffusion of heat. This can also be predicted in the context of the augmentation in the kinetic energy while the Eckert number increases.It is also considerably observed in Fig. 7 that the heat distribution profile elevates significantly with the radiation parameter as the absorbed energy by the fluid due to this factor contributes to heating up the whole system. In Fig. 8 it has been noticed that enhancing the value of the heat source parameter (Q), the thermal profile reduces due to the dominance of thermal dissipation mechanisms.

The impact of the Brownian motion factor (Nb) on both the thermal and concentrationprofiles is portrayed in Figs 9 and 10. The augmentation in the thermal distribution profile can be justified with an increment in the Brownian motion factor as it is the

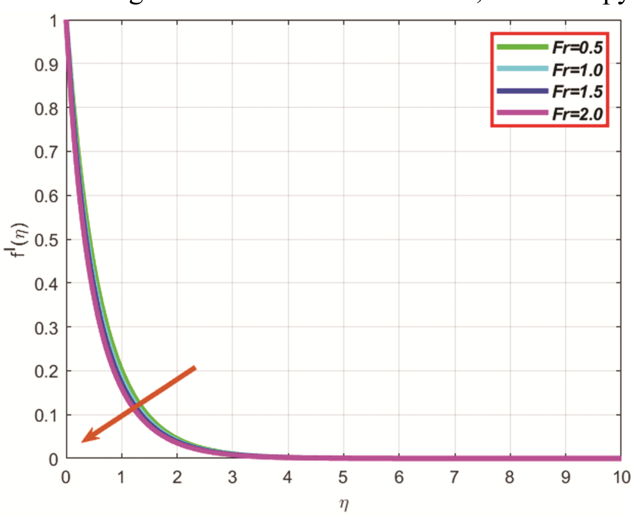

Fig. 5 — Plot of $f'(\eta)$ with various values of Fr

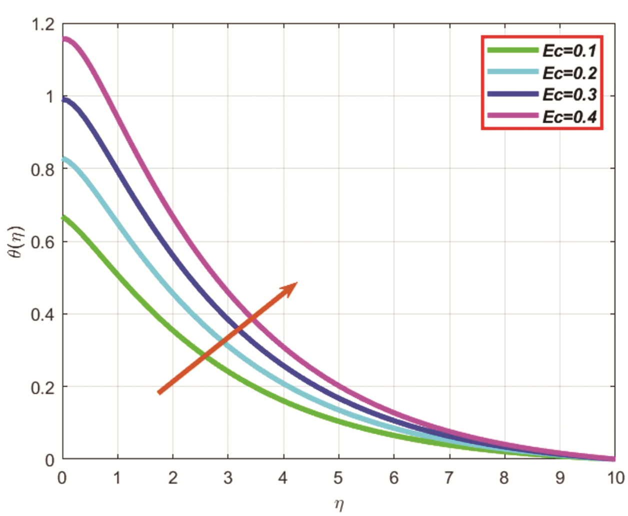

Fig. 6 — Plot of $\theta(\eta)$ with various values of Ec

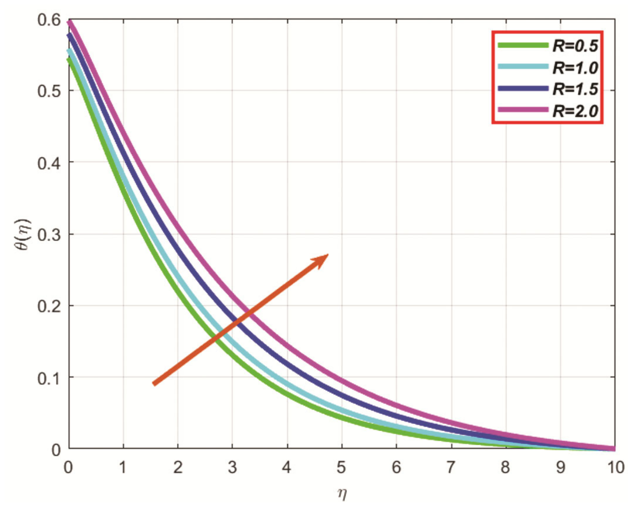

Fig. 7 — Plot of $\theta(\eta)$ with various values of R

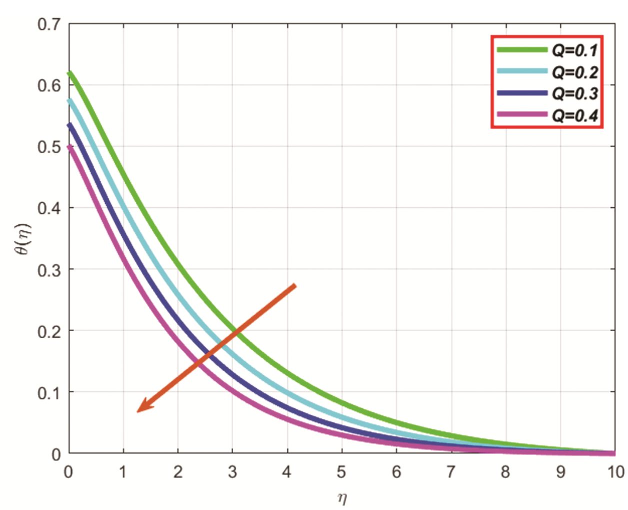

Fig. 8 — Plot of $\theta(\eta)$ with various values of Q

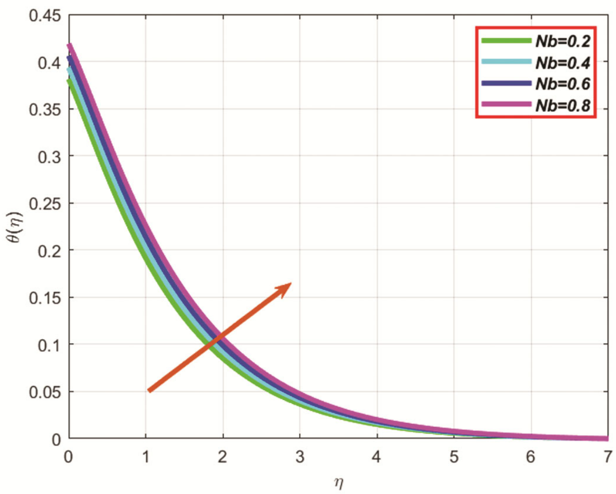

Fig. 9 — Plot of $\theta(\eta)$ with various values of *Nb*

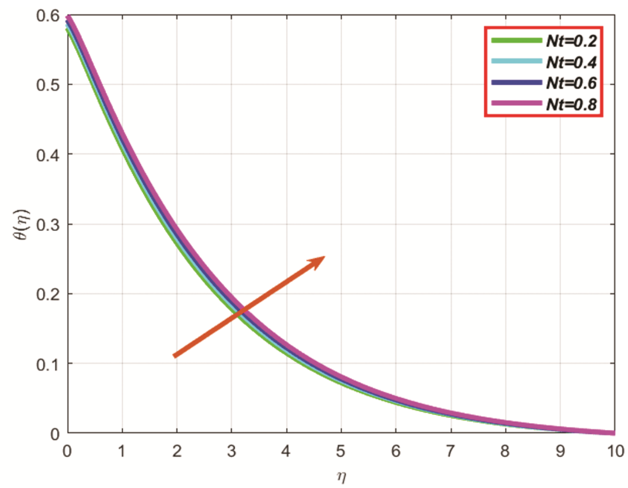

Fig. 11 — Plot of $\theta(\eta)$ with various values of *Nt*

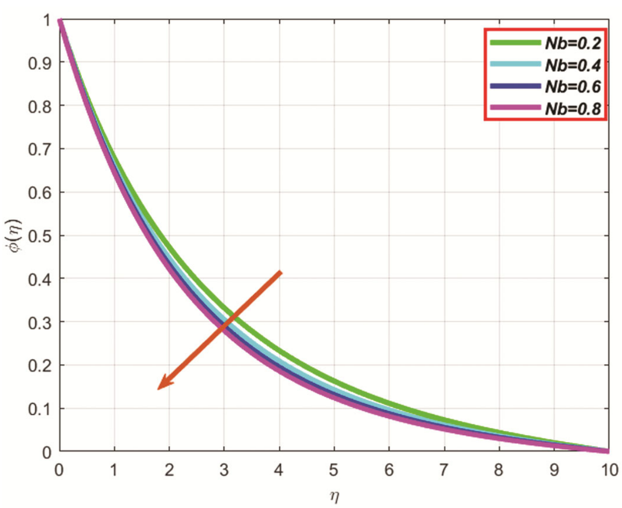

Fig. 10 — Plot of $\phi(\eta)$ with various values of *Nb*

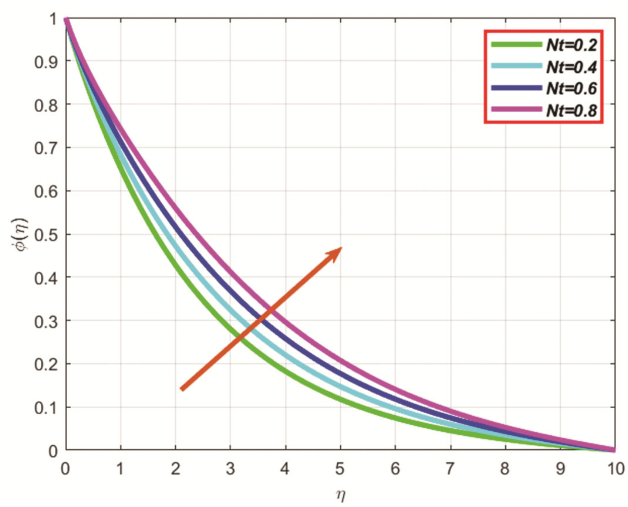

Fig. 12 — Plot of $\phi(\eta)$ with various values of *Nt*

key factor of the erratic motion of the fluid's particles. Thus, a highly conspicuous thermal distribution curve develops as a consequence of the exaggerated mingling and transmission of heat instigated by this enhanced Brownian gesture. Furthermore, as demonstrated in Fig. 10, a prompt reduction associated with the concentration profile is noted with an elevated Brownian motion factor (Nb). Since enhanced random mobility of nanoparticles due to augmented Brownian motion results in amplified dispersion. A decrease in the concentration profile results from this enhanced diffusion.The impact of the thermophoresis factor on thermal distribution and concentration distribution profile is portrayed in Figs 11 and 12, respectively. In a system associated with a greater Nt, the thermal distribution profile arises as a conspicuous amount of fluid is transported from a heated region to a cold region. In this instance, the thermophoresis effect triggered by the thermal gradient initiates an expeditious cum easy flow, along the stretched surface. It therefore implies that as Nt elevates, the concentration distribution profile also improves significantly.

In Fig. 13, an inverse connection between the Schmidt number (Sc) and the concentration curve is demonstrated. As the Schmidt number escalates, there is a noticeable reduction in the concentration profile. This phenomenon arises due to the higher rate of momentum diffusion relative to mass diffusion associated with the enhancing Schmidt number. Consequently, there is an accelerated dispersion of momentum compared to mass within the fluid flow system. This disparity in diffusion rates results in a

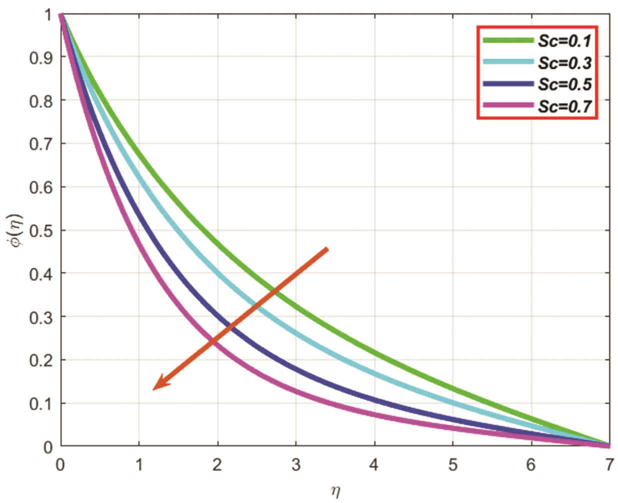

Fig. 13 — Plot of $\phi(\eta)$ with various values of *Sc*

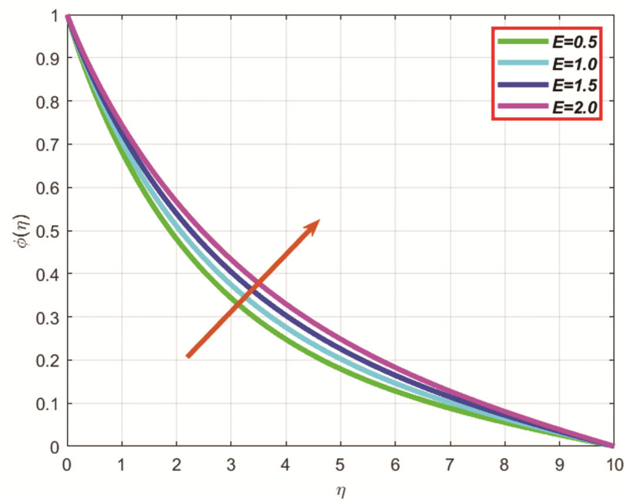

Fig. 15 — Plot of $\phi(\eta)$ with various values of *E*

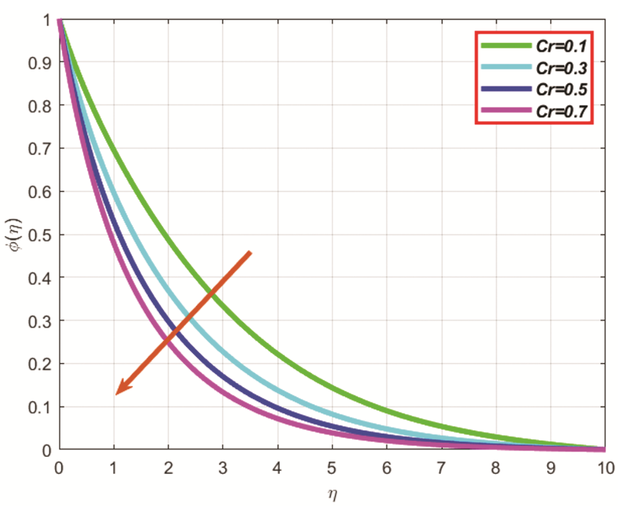

Fig. 14 — Plot of $\phi(\eta)$ with various values of *Cr*

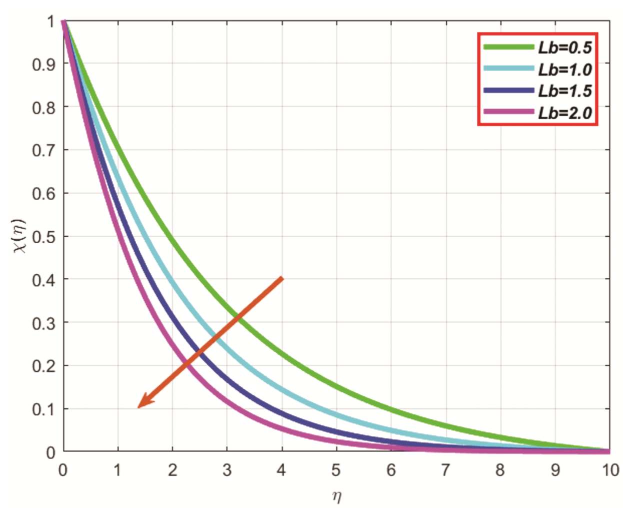

Fig. 16 — Plot of $X(\eta)$ with various values of *Lb*

less pronounced concentration gradient, ultimately leading to the reduction of the concentration curve. Enlarging the chemical reaction factor (Cr) induces a declination in the concentration curve, as indicated in Fig. 14. This effect develops from the heightened pace of reaction catalyzed by Cr, prompting the rapid consumption of reactants. Consequently, the concentration of reactants reduces, enhancing a shallower concentration gradient over the system. The rise in the activation energy factor (E) illustrated in Fig. 15 results in an escalation of the concentration profile, attributed to its impact on the reaction kinetics. Enhanced activation energy imposes a higher energy barrier for reactant molecules, impeding their conversion into products and decelerating the reaction rate. Consequently, reactants persist for longer durations within the system, fostering a more pronounced concentration gradient.

As depicted in Fig. 16, a reduction is observed for enlarging the value of Bioconvection Lewis number (Lb) on the motile microorganism profile. Physically, accelerating the Bioconvection Lewis number results in a reduced motile microorganism profile due to the concurrent declination in their diffusive capacity relative to the fluid flow. Also, as depicted in Fig. 17, a reduction is noticed for enlarging the value of the Peclet number (Pe). Physically, escalating the Peclet number (Pe) leads to a decreased motile microorganism profile due to the prevalence of convective transport over diffusive transport. In Fig. 18, the same pattern is noticed for the Bioconvection constant (δ_1) against

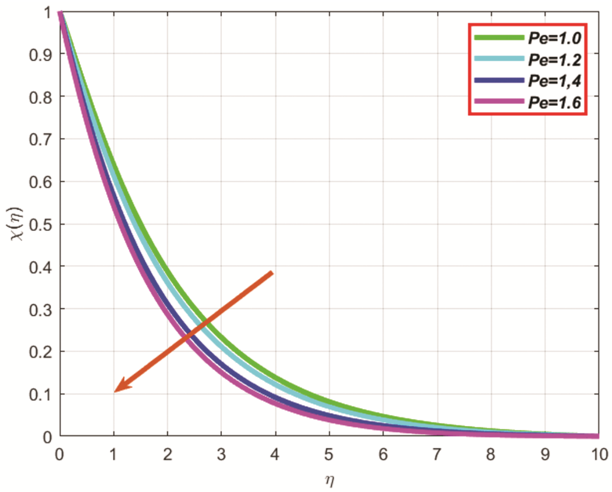

Fig. 17 — Plot of $X(\eta)$ with various values of Pe

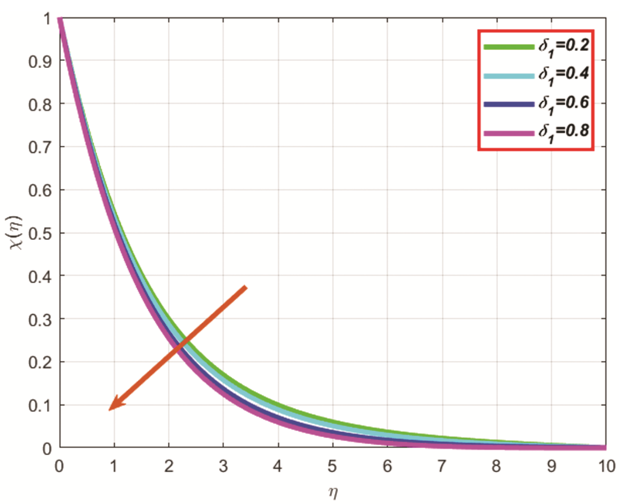

Fig. 18 — Plot of $X(\eta)$ with various values of δ_1

the motile microorganism profile. That is escalating the values of δ_1, reduces the motile microorganism curve. Stronger bioconvection factors endorse microorganism mixing, averting accumulation and causing a decay in the motile microorganism profile.

In Fig. 19, the connection between the suction factor (S) and velocity is demonstrated. As the suction factor escalates, there is a discernible decrease in the velocity profile. This phenomenon is attributed to the enhanced strength of suction forces associated with higher suction parameter values. These intensified suction forces exert a more pronounced pull on the fluid, compelling it toward the surface with greater vigor. Consequently, the fluid velocity diminishes as a larger volume of fluid is drawn toward the surface, resulting in a declination of the velocity curve reported within the system.

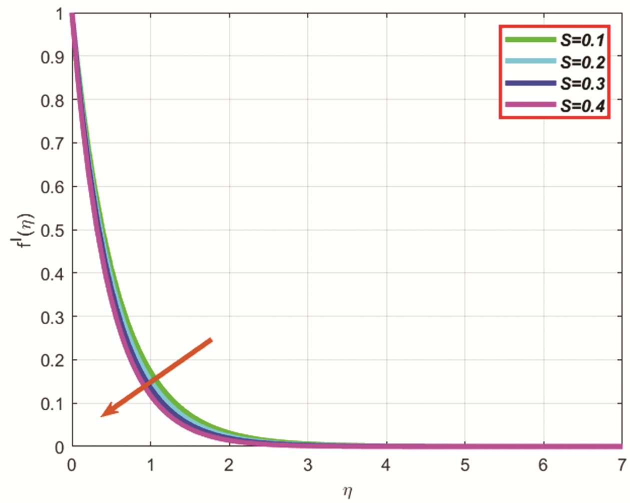

Fig. 19 — Plot of $f'(\eta)$ with various values of S

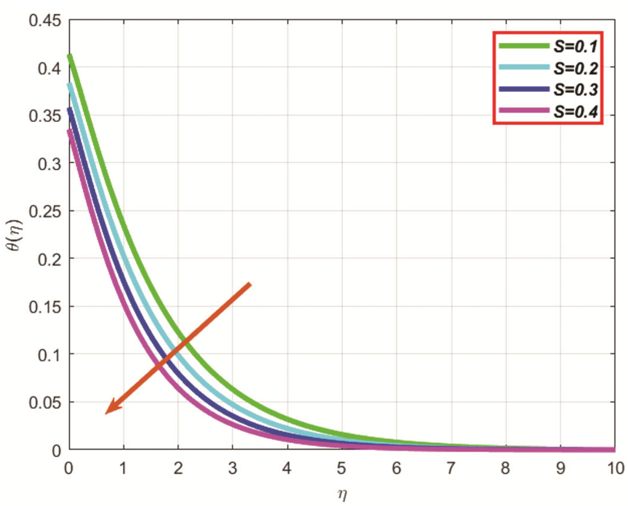

Fig. 20 — Plot of $\theta(\eta)$ with various values of S

Moreover, in Fig. 20, the correlation between the suction factor (S) and the heat profile is displayed. As the suction parameter boosts, a remarkable reduction in the thermal profile is observed. This phenomenon stems from the amplification of convective thermal transport, which is facilitated by larger suction factor values. This augmentation in convective thermal transfer escalates the efficacy of thermal dissipation from the system. Consequently, the temperature gradient diminishes as a higher quantity of heat is effectively extracted from the system due to enhanced suction. This results in a reduction in the thermal profile, indicating the gradual removal of heat from the system.The thermal curve is boosted for escalating values of the Biot number (Bi) as indicated in Fig. 21. Physically, enhanced Biot numbers denote slower

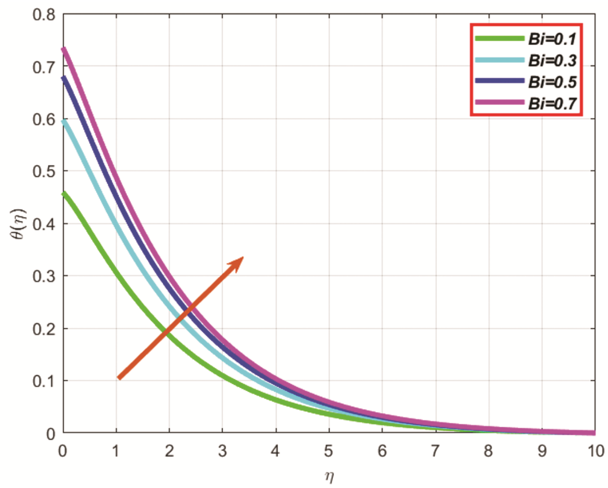

Fig. 21 — Plot of $\theta(\eta)$ with various values of Bi

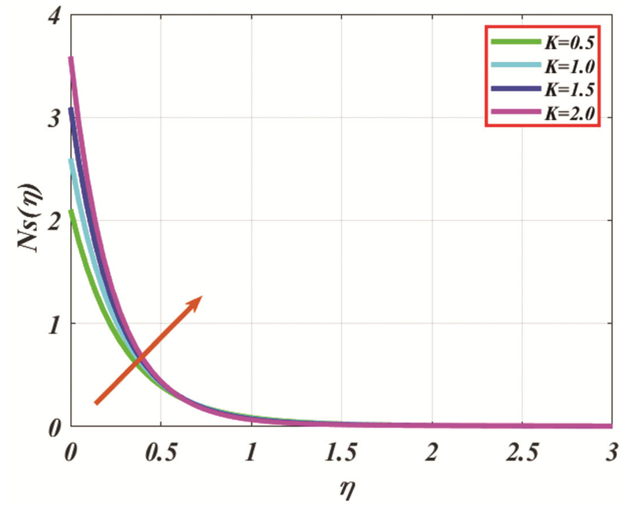

Fig. 23 — Plot of Ns (η) with various values of K

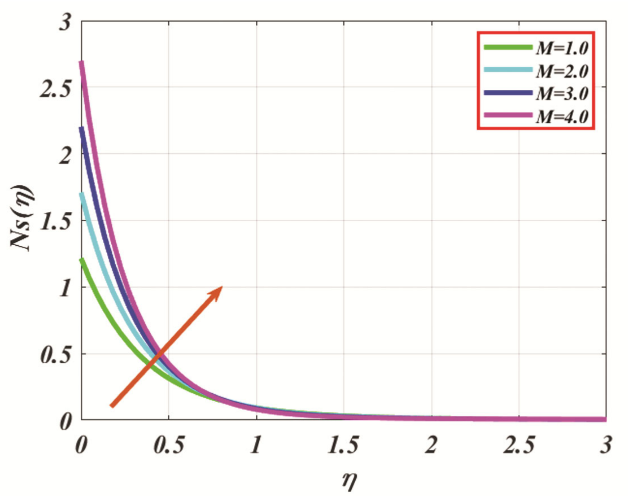

Fig. 22 — Plot of Ns (η) with various values of M

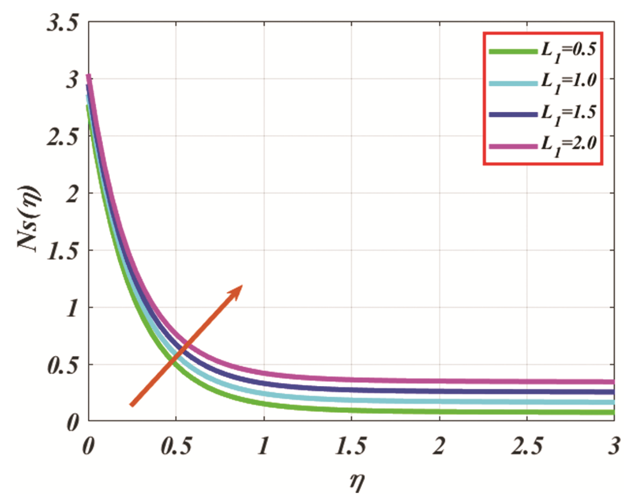

Fig. 24 — Plot of Ns (η) with various values of L_1

thermal transport within a solid compared to its surface. This disparity results in less efficient thermal conduction within the solid, leading to a thicker heat boundary layer. Consequently, an escalated Biot number correlates with an expanded heat profile due to diminished thermal transfer efficiency within the solid medium.

An elevation in entropy generation distribution is noticed for augmenting the value of magnetic factor (M) in Fig. 22. Physically, the enhanced magnetic factor induces the Lorentz force, which increases viscous dissipation and joule heating in the field. These influences enhance irreversibility, leading to elevating entropy generation. Also, as the porosity factor (K) elevates the entropy generation curve also escalates, as depicted in Fig. 23. The elevation of the porosity factor (K) amplifies fluid flow within the porous medium, thereby escalating mixing processes and subsequently leading to an enhancement in entropy generation within the system. In Fig. 24, the diffusion parameter (L_1) is enhanced, and the entropy generation profile also escalates due to the heightened molecular diffusion associated with larger L_1 values. This amplification in molecular diffusion fosters more extensive mixing processes, consequently leading to a more pronounced enhancement in entropy generation within the system. In Fig. 25, the relationship between the temperature difference parameter (α_1) and entropy generation is elucidated. As the temperature difference factor enhances, there is a concurrent escalation in entropy generation. Thermal gradients become more intense as the temperature difference factor rises, growing the irreversibilities of thermal transport. Because of amplified energy

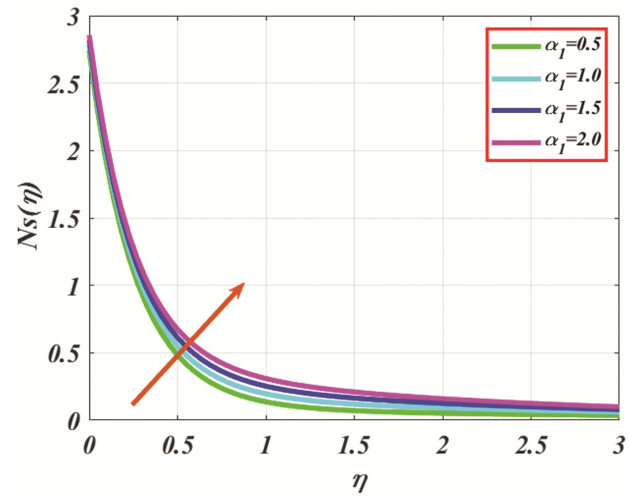

Fig. 25 — Plot of Ns (η) with various values of α_1

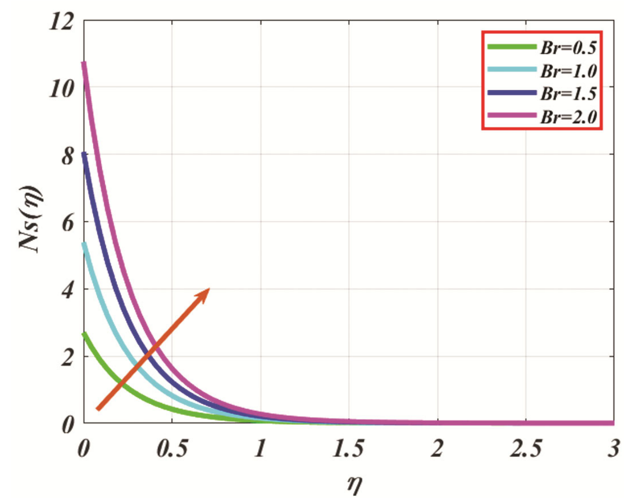

Fig. 26 — Plot of Ns (η) with various values of Br

dissipation and thermodynamic disturbance, this upsurges entropy generation. Also, in Fig. 26, the connection between the Brinkman number (Br) and entropy generation is illustrated. As the Brinkman number enhances, there is a concurrent growth in entropy generation. This phenomenon stems from the amplified viscous dissipation occurring within the fluid flow at larger Brinkman numbers. Consequently, an enhanced proportion of mechanical energy is transformed into heat, contributing to heightened entropy generation within the system.

As demonstrated in Table 1, The skin friction coefficient is reckoned to be ameliorated with the fortified effect of Lorentz force, porosity followed by Forchheimer impact, and suction velocity whereas, the Williamson fluid factor effect demoted the rate of shear stress at the vicinity. Moreover, Table 2 has been prepared to delineate the variation in thermal transmission rate for various prompt factors. Prandtl number (Pr), Radiation (R), and heat source factor (Q) alongside suction (S) and Biot number (Bi) significantly touched up the thermal efficacy rate in the proximity of the surface. On the other hand, Eckert number (Ec), Brownian motion factor (Nb) and Thermophoresis factor (Nt) exhibit a reverse pattern in the context of the thermal transmission rate.

Table 1 — Variations in skin friction for various parameter values

M	K	We	Fr	S	$C_f(Re_x)^{\frac{1}{2}}$
1.0					-1.477742
2.0					-1.758635
3.0					-1.996164
	0.5				-1.857811
	1.0				-1.973876
	1.5				-2.082577
		0.1			-1.758635
		0.2			-1.511875
		0.3			-0.975480
			0.5		-1.787103
			1.0		-1.855624
			1.5		-1.920718
				0.1	-1.758635
				0.2	-1.801445
				0.3	-1.845063

Table 2 — Variations in rate of heat transfer for various parameter values

Pr	R	Q	Ec	Nb	Nt	S	Bi	$(Re_x)^{-\frac{1}{2}}Nu$
0.7								0.200651
0.8								0.209637
0.9								0.217624
	0.5							0.214126
	1.0							0.268170
	1.5							0.319090
		0.1						0.168289
		0.2						0.186183
		0.3						0.202533
			0.1					0.202533
			0.2					0.157159
			0.3					0.111471
				0.2				0.210720
				0.4				0.205288
				0.6				0.199752
					0.2			0.205698
					0.4			0.203600
					0.6			0.201454
						0.1		0.202533
						0.2		0.215301
						0.3		0.227063
							0.1	0.098279
							0.2	0.202533
							0.3	0.256363

Table 3 — Variations in rate of mass transfer for various parameter values

Sc	Cr	Nb	Nt	E	$(Re_x)^{-\frac{1}{2}} Sh$
0.1					0.081285
0.3					0.204540
0.5					0.319531
	0.1				0.204540
	0.3				0.331816
	0.5				0.425054
		0.2			0.080851
		0.4			0.183881
		0.6			0.218341
			0.2		0.246190
			0.4		0.218072
			0.6		0.191366
				0.5	0.178927
				1.0	0.156203
				0.5	0.141155

Table 4 — Variations in the rate of motile density number for various parameter values

Lb	Pe	δ_1	$\frac{Nh}{\sqrt{Re_x}}$
0.5			0.433115
1.0			0.645337
1.5			0.838304
	1.0		0.679127
	1.2		0.712947
	1.4		0.746807
		0.2	0.645337
		0.4	0.665762
		0.6	0.686187

However, as exhibited in Table 3, the significant impacts of Schmidt number (Sc), chemical reaction parameter (Cr), Brownian motion factor (Nb), Thermophoresis factor (Nt), and Arhhenius energy (E) on mass transmission rate is portrayed. The upsurge variation in Sherwood number is noted with Sc, Cr, and Nb while the scenario is vice versa with Nt and E.Because augmented values of Sc reduce mass diffusivity, Cr accelerates species consumption, and Nb augments nanoparticle diffusion, all endorsing mass transfer. Also, higher Nt drives nanoparticles away from higher concentration regions, and higher Edeclines reaction rates, dropping mass transport efficiency.Again, the variation in the rate of motile density number is improved with Bioconvection Lewis number (Lb), Peclet number (Pe), and Bio convection constant (δ_1) as shown in Table 4.

Conclusion

This numerical investigation undertakes a comprehensive investigation of the Williamson bioconvective nanofluid flow incorporating the Entropy generation in Darcy Forchheimer medium across a stretching sheet along with the motile microorganisms and activation energy impacts. It also meticulously considers the impacts of suction/injection, Brownian motion, thermophoresis, chemical reaction, Newtonian boundary heating, and heat source. Computational outcomes are obtained by Runge-Kutta based shooting technique via the BVP5C MATLAB package. The noteworthy findings are demonstrated as follows:

- The escalation in Brinkman number leads to a simultaneous enhancement in entropy generation, driven by intensified viscous dissipation in fluid flow, which converts a greater portion of mechanical energy into heat, thereby heightening entropy within the system.
- The motile microorganism profile reduces for enlarging values of $Lb, Pe,$ and δ_1. Also, fluid velocity is enhanced for escalating $Fr, S, K,$ and M.
- As the temperature difference factor (L_1) and diffusion parameter due to concentration (α_1) enhances, along with the elevation of the porosity factor (K) and magnetic factor (M), there is a concurrent escalation in entropy generation.
- An upsurge in the magnitudes of Eckert Number (Ec). Radiation factor (R), Thermophoresis factor (Nt), Brownian motion term (Nb) and Biot number (Bi) escalated the thermal curve. While suction term shows the opposite trend.
- The Prandtl number (Pr), Radiation (R), and heat source factor (Q) alongside suction (S) and Biot number (Bi) significantly touched up the thermal efficacy rate in the proximity of the surface.
- Enlarging the magnitudes of activation energy factor escalates the concentration curve. Also, the proximity solutal transfer rate exhibits elevation with escalating$Sc,\ Cr$, and Nb while the scenario is vice versa with $Nt$and E.
- The variation in motile density number is elevated with Bioconvection Lewis number (Lb), Peclet number (Pe), and Bio convection constant (δ_1).

This study may be expanded in the future by exploring three-dimensional and unsteady influences on Williamson bioconvective nanofluid flow. Understanding may be improved by looking at non-Newtonian models in porous media with distinct rheological features. Furthermore, entropy generation analysis may be optimized by machine learning approaches.

Nomenclature

Letters

B_o Uniform magnetic field (kg/S^2A)
Bi Biot number
Cr Chemical reaction parameter
D_B Brownian diffusion coefficient
D_T Thermophoresis diffusion coefficient
Ec Eckert number
Fr Darcy Forchheimer
K_r Rate of reaction constant
K Porosity parameter
Lb Bioconvection Lewis number
M Magnetic field
Nb Brownian motion
Nt Thermophoresis parameter
Nu Nusselt number
Nh Motile density number
Pe Peclet number
Pr Prandtl number
Q Heat source parameter
R Radiation parameter
S Suction parameter
Sc Schmidt number
Sh Sherwood number
T_∞ Free stream temperature (K)
u, v Velocity components in x and y directions (m/s)
We Williamson fluid parameter
x, y Cartesian coordinates (m)

Greek symbols

δ_1 Bioconvection constant
ρ Fluid density (kg/m^3)
ρC_p Fluid thermal capacity (J/m^3K)
υ Kinematic viscosity (m^2/s)
μ Dynamic viscosity $(kg/(ms))$

References

1 Choi S U & Eastman J A, Enhancing thermal conductivity of fluids with nanoparticles (No. ANL/MSD/CP-84938; CONF-951135-29). Argonne National Lab, (ANL), Argonne, IL (United States) (1995).
2 Khan U A, Ahmed N, Mohyud-Din S T, Alsulami M D & Khan I, A novel analysis of heat transfer in the nanofluid composed by nanodimaond and silver nanomaterials: Numerical investigation, *Sci Rep*, 12 (2022) 1284.
3 Abbas N, Tumreen M, Shatanawi W, Qasim M & Shatnawi T A, Thermodynamic properties of second grade nanofluid flow with radiation and chemical reaction over slendering stretching sheet, *Alex Eng J*, 70 (2023) 219.
4 Paul A, Nath J M & Das T K, An investigation of the MHD Cu-Al_2O_3/H_2O hybrid-nanofluid in a porous medium across a vertically stretching cylinder incorporating thermal stratification impact, *J Therm Eng*, 9 (2023) 799.
5 Ahmad B, Idrees M, Shah S A A, Nisar K S & Abdel-Aty A H, A study on the impact of solar radiations and activation energy effects in existence of nanofluid over stretching solar sheets, *Case Stud Therm Eng*, 59 (2024) 104448.
6 Ali F, Zaib A, Padmavathi T, Faizan M & Zafar S S, Exact solution of radiative flow on the mixed convection flow of Hybrid Nanofluid in a porous medium; Laplace transform technique for sustainable energy, *Surface Rev Lett*, (2024).
7 Shah N A, Ali F, Yook S J, Faizan M, Zafar S S & Sidi M O, Dynamics of chemical reactive on magneto hybrid nanomaterial with heat radiation due to porous exponential plate: Laplace transform technique for the heat and mass, *J Radiat Res Appl Sci*, 18 (2025) 101295.
8 Asjad M I, Zahid M, Inc M, Baleanu D & Almohsen B, Impact of activation energy and MHD on Williamson fluid flow in the presence of bioconvection, *Alex Eng J*, 61 (2022) 8715.
9 Saravana R, Hemadri R R, Narasimha M K V & Makinde O D, Thermal radiation and diffusion effects in MHD Williamson and Casson fluid flows past a slendering stretching surface, *Heat Transf*, 51 (2022) 3187.
10 Khan K A, Javed M F, Ullah M A & Riaz M B, Heat and Mass transport analysis for Williamson MHD nanofluid flow over a stretched sheet, *Results Phys*, 53 (2023) 106873.
11 Jangid S, Mehta R, Bhatnagar A, Alotaibi M F & Ahmad H, Heat and mass transfer of hydromagnetic Williamson nanofluid flow study over an exponentially stretched surface with suction/injection, buoyancy, radiation and chemical reaction impacts, *Case Stud Therm Eng*, 59 (2024) 104278.
12 Sharma B K & Gandhi R, Combined effects of Joule heating and non-uniform heat source/sink on unsteady MHD mixed convective flow over a vertical stretching surface embedded in a Darcy-Forchheimer porous medium, *Propuls Power Res*, 11 (2022) 276.
13 Jawad M, Majeed A H, Nisar K S, Hamida M B B, Alasiri A, Hassan A M & Sharshir S W, Numerical simulation of chemically reacting Darcy-Forchheimer flow of Buongiorno Maxwell fluid with Arrhenius energy in the appearance of nanoparticles, *Case Stud Therm Eng*, 50 (2023) 103413.
14 Zafar S S, Khan U, Ali F, Eldin S M, Saeed A M, Zaib A & Galal A M, Irreversibility analysis of radiative flow of Prandtl nanofluid over a stretched surface in Darcy-Forchheimer medium with activation energy and chemical reaction. *Heliyon*, 9 (2023) e14877.
15 Awais M, Salahuddin T & Muhammad S, Effects of viscous dissipation and activation energy for the MHD Eyring-powell fluid flow with Darcy-Forchheimer and variable fluid properties, *Ain Shams Eng J*, 15 (2024) 102422.
16 Haq F, Kadry S, Chu Y M, Khan M & Khan M I, Modeling and theoretical analysis of gyrotactic microorganisms in radiated nanomaterial Williamson fluid with activation energy, *J Mater Res Technol*, 9 (2020) 10468.
17 Song Y Q, Khan S U, Khan M I, Awais M, Abbasi A & Shi Q H, Bidirectional non-linear stretched flow of

Williamson nanofluid with swimming of motile gyrotactic microorganisms, *Appl Math Comput*, 411 (2021) 126502.
18 Awan A U, Shah S A A & Ali B, Bio-convection effects on Williamson nanofluid flow with exponential heat source and motile microorganism over a stretching sheet, *Chin J Phys*, 77 (2022) 2795.
19 Hussain Z, Khan W A, Ali M, Waqas M & Ashraf I M, Chemically reactive magneto-bioconvection 3D flow of radiative Williamson nanofluid containing oxytactic moment of microorganisms, *Tribol Int*, 189 (2023) 108934.
20 Kamal M, Ali F, Khan N, Faizan M, Gul N, Muhammad T & Kolsi L, Second law analysis of two phase Maxwell mixed convective nanofluid using Marangoni flow and gyrotactic microorganism framed by rotating disk, *J Therm Anal Calorim*, (2025) 1.
21 Hamid A & Khan M, Impacts of binary chemical reaction with activation energy on unsteady flow of magneto-Williamson nanofluid, *J Mol Liq*, 262 (2018) 435.
22 Dhlamini M, Kameswaran P K, Sibanda P, Motsa S & Mondal H, Activation energy and binary chemical reaction effects in mixed convective nanofluid flow with convective boundary conditions, *J Comput Des Eng*, 6 (2019) 149.
23 Khan M I, Alsaedi A, Qayyum S, Hayat T & Khan M I, Entropy generation optimization in flow of Prandtl–Eyring nanofluid with binary chemical reaction and Arrhenius activation energy, *Colloids Surfaces A: Physicochem Eng Asp*, 570 (2019) 117.
24 Vijayalakshmi K, Chandulal A, Alhazmi H, Aljohani A F & Khan I, Effect of chemical reaction and activation energy on Riga plate embedded in a permeable medium over a Maxwell fluid flow, *Case Stud Therm Eng*, 59 (2024)104457.
25 Kumar A, Tripathi R, Singh R & Chaurasiya V K, Simultaneous effects of nonlinear thermal radiation and Joule heating on the flow of Williamson nanofluid with entropy generation, *Phys A: Stat Mech Appl*, 551 (2020) 123972.
26 Butt A S, Ali A & Mehmood A, Numerical investigation of magnetic field effects on entropy generation in viscous flow over a stretching cylinder embedded in a porous medium, *Energy*, 99 (2016) 237.
27 Baag S, Mishra S R, Dash G C & Acharya M R, Entropy generation analysis for viscoelastic MHD flow over a stretching sheet embedded in a porous medium, *Ain Shams Eng J*, 8 (2017) 623.
28 Khan M I, Qayyum S, Hayat T, Waqas M, Khan M I & Alsaedi A, Entropy generation minimization and binary chemical reaction with Arrhenius activation energy in MHD radiative flow of nanomaterial, *J Mol Liq*, 259 (2018) 274.
29 Ullah Z, El-Zahar E R, Aldhabani M S, Alrihieli H F & Seddek L F, Heat transfer assessment with entropy generation and thermal density effects on boundary layer flow of magneto nanofluid across the stretching sheet under magnetic field, *Therm Sci Eng Prog*, 43 (2023) 101955.
30 Hussain S, Haq F, Ghazwani H A, Saleem M & Hussain A, Entropy optimization in bio-convective chemically reactive flow of micropolar nanomaterial with activation energy and gyrotactic microorganisms, *Case Stud Therm Eng*, 55 (2024) 104131.
31 Algehyne E A, Alamrani F M, Lone S A, Ali F, Saeed A & Khan A, Numerical exploration of radiative heat transfers in a magneto bioconvection Maxwell fluid passing through a spinning disk, *Adv Mech Eng*, 16 (2024) 16878132241282017.
32 Ali F, Zaib A, Sidi M O & Khan U, Irreversibility analysis of bio-convection nanofluid flow in a Darcy-Forchheimer porous medium induced by a rotating disk with thermal radiation, *J Radiat Res Appl Sci*, 18 (2025) 101273.
33 Zafar S S, Zaib A, Faizan M, Shah N A, Ali F & Yook S J, Bioconvection flow of Prandtl nanomaterial due to stretched cylinder enclosed through Darcy Forchheimer flow with triple stratification, *Alex Eng J*, 116 (2025) 188.